

Development of a Near-Infrared Echelle Spectrograph “NICE”

Tomoyasu YAMAMURO,^{1,2*} Hironobu KAWABATA,^{1,3} Ko NEDACHI,^{1,4} Yuichiro NISHIMAKI,¹
Kentaro MOTOHARA,¹ Takashi MIYATA,¹ Tae-Soo PYO,^{1,4} Norihide TAKEYAMA,^{1,2}
and Masuo TANAKA¹

¹*Institute of Astronomy, The University of Tokyo, 2-21-1 Osawa, Mitaka, Tokyo 181-0015*

²*Genesia corporation, 3-38-4-601 Shimorenjaku, Mitaka, Tokyo 181-0013*

³*Musashi High School, 1-26-1 Toyotama-kami, Nerima, Tokyo 176-8535*

⁴*Subaru Telescope, National Astronomical Observatroy of Japan, 650 North A’ohoku Place, Hilo, HI 96720, U.S.A.
tyamamur@ioa.s.u-tokyo.ac.jp*

(Received 2006 September 1; accepted 2006 December 13)

Abstract

We developed a Near-Infrared Cross-dispersed Echelle spectrograph, “NICE”, which covers the wavelength range from $0.9\ \mu\text{m}$ to $2.4\ \mu\text{m}$ with four exposures, and has a wavelength resolution of $\lambda/\delta\lambda \sim 2600$. These capabilities enable us to simultaneously evaluate the continuum level and intensity of various lines of a spectrum with high accuracy over a wide wavelength range. Since NICE is designed to be compact, by adopting a “white pupil” configuration and fully refractive lenses, we can carry out observations with small telescopes.

Key words: instrumentation: spectrographs

1. Introduction

A Near-Infrared Cross-dispersed Echelle spectrograph, “NICE”, was developed for investigating mass-loss phenomena of mainly massive stars in the post-main-sequence phase, e.g., supergiants, Wolf-Rayet stars (Y. Nishimaki et al. 2006, in preparation), luminous blue variables (LBV), and yellow hypergiants (Yamamuro et al. 2006a). These stars show photospheric continua with many absorption and emission lines of atoms and molecules, and sometimes circumstellar dust emission in the near-infrared wavelength range. NICE was designed to cover the wavelength range from $0.9\ \mu\text{m}$ to $2.4\ \mu\text{m}$ corresponding to almost the whole sensitive range of HgCdTe detectors. The wavelength resolution, $R \equiv \lambda/\delta\lambda$, was designed to be ~ 2600 so as to resolve many lines, and also to obtain velocity profiles of lines for post-main-sequence massive stars. Moreover, the resolution of $R \sim 2600$ enables us to resolve and remove telluric OH lines, whose typical wavelength separation, $\Delta\lambda$, corresponds to $\lambda/\Delta\lambda \lesssim 1000$ (Oliva & Origlia 1992; Maihara et al. 1993; Rousselot et al. 2000).

NICE was designed to be compact and light weight in order to carry out observations for long-term monitoring with small- or middle-size telescopes. The optical parameters are optimized to the 1.5 m infrared telescope ($D = 1.5\ \text{m}$, $F = 12.2$) of National Astronomical Observatory of Japan (NAOJ) in Tokyo, while NICE can be installed to other telescopes by adding F-conversion lenses for the optimum throughput.

We describe the basic design of NICE in section 2, the performance in section 3, and show examples of astronomical data in section 4.

2. Development

2.1. Optical System

The optical system of NICE was designed as a cross-dispersed echelle spectrograph, adopting a semi-Littrow configuration for an echelle grating, a “white pupil” configuration (Barnne et al. 1996) between the echelle and a cross-disperser, and fully refractive lenses. The whole optical layout and the spot-diagrams are shown in figures 1 and 2, respectively. The principal optical parameters and the device specifications are summarized in tables 1 and 2, respectively. We describe the design approach in the following.

2.1.1. Specifications

The wavelength coverage was decided to be almost the whole sensitive range of NICMOS-3 (see subsection 2.3), i.e., $0.9\text{--}2.4\ \mu\text{m}$. In order to cover this range with resolution for 2 pixels of the detector ($R_{2\text{pix}}$) of ~ 2600 ($\delta v \sim 110\ \text{km s}^{-1}$), the whole wavelength range was divided into four ranges: $0.91\text{--}1.20\ \mu\text{m}$ (designated as “I frame” or simply I), $1.17\text{--}1.47\ \mu\text{m}$ (J), $1.41\text{--}1.78\ \mu\text{m}$ (H), and $1.73\text{--}2.45\ \mu\text{m}$ (K). Note that the neighboring ranges overlap at the wavelengths of atmospheric windows to obtain a continuous spectrum with no break by connecting the four ranges. The echelle formats, the wavelength ranges and the diffraction efficiency of the echelle with the cross-disperser are shown in figure 3 together with the atmospheric transmittance. To avoid degradation of $R_{2\text{pix}}$ by the broader slits, we adopted two selectable narrow slits, whose widths correspond to 0.75 pixel and 1.5 pixel, i.e., $30\ \mu\text{m}$ and $60\ \mu\text{m}$ on the detector, respectively. The degradation of the photometric accuracy due to under sampling with the narrower slits is recovered by observing standard stars right before or after each target star while the configuration of NICE is kept (see section 4). The slit widths on the sky were chosen to be $1''$ and $2''$, which correspond to $90\ \mu\text{m}$ and $180\ \mu\text{m}$ on the focal plane of the 1.5 m telescope, respectively, because the typical

* Current affiliation is OptCraft, 67 Horinishi, Hadano, Kanagawa 259-1331.

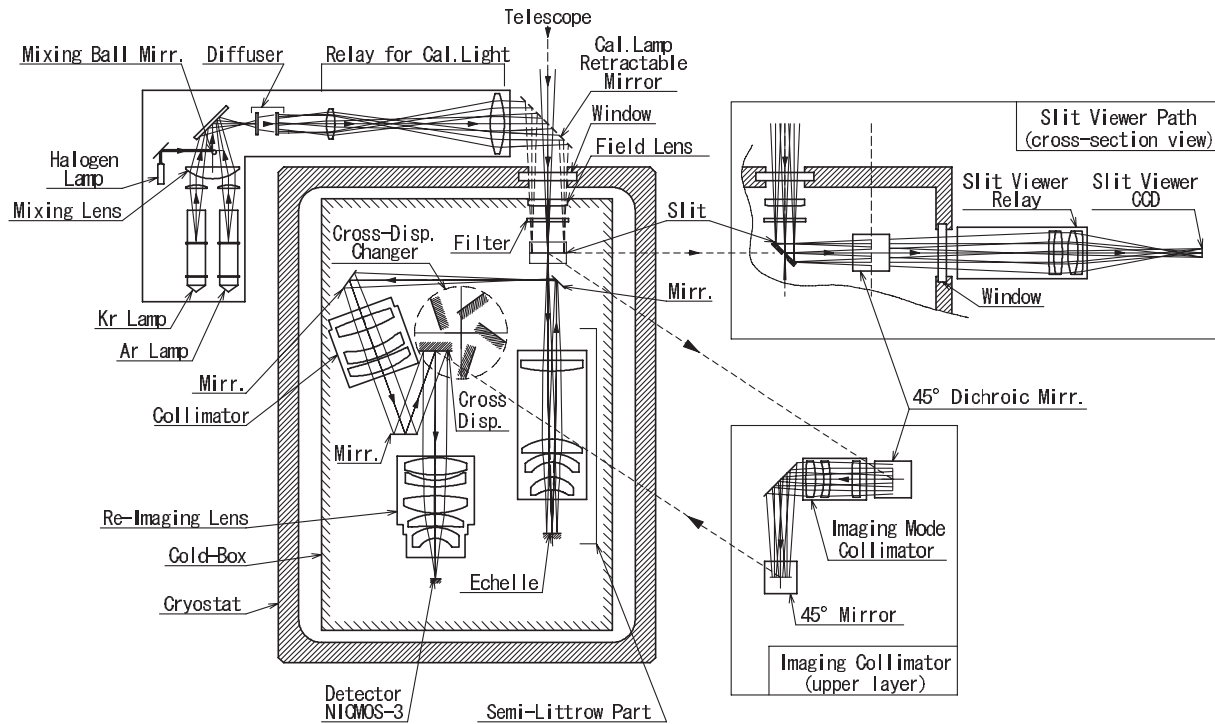


Fig. 1. Structure and optical layout of NICE. A ray coming from the telescope passes through the window, the field lens, the filter, and focuses on the slit. The ray passing through the slit is dispersed perpendicularly to this plane by an echelle in the semi-Littrow part, and focused near the slit again. The ray is collimated by the collimator, dispersed in this plane by the cross-disperser, and focused on the detector by the re-imaging lens. See subsection 2.1.4 for details on the calibration lamps, the slit viewer, and the infrared-imaging mode.

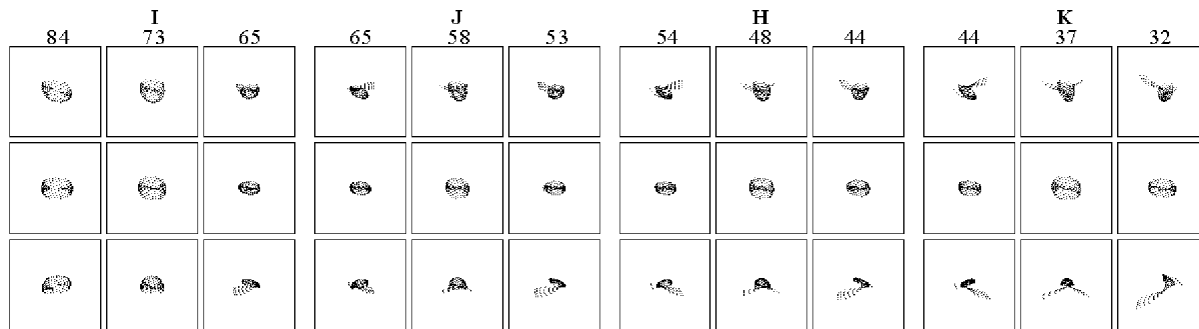


Fig. 2. Spot diagrams at different 36 wavelengths in the spectroscopic mode. Their positions on the detector are marked in the upper panels of figure 3 with circles. Numbers given at the top mean the echelle orders. Each square corresponds to one pixel size of NICMOS-3 ($40\ \mu\text{m}$).

seeing size is $1''\text{--}2''$ at the site in Tokyo. In order to realize the above specifications for NICE, the optical system was designed as described in subsections 2.1.2–2.1.3.

2.1.2. Semi-littrow configuration and white pupil configuration

The above specifications required us to make a semi-Littrow configuration and a white pupil configuration in the optical design for the following reasons: (1) The angle γ to the echelle grating distorts and rotates the slit image on the detector; here, γ is the half angle between the incident and exit rays in the plane perpendicular to the echelle dispersion (Schroeder 2000). A smaller γ can make the distortion and rotation smaller. The γ value can be certainly designed to be smaller in a Littrow or semi-Littrow configuration. (2) The white pupil configuration

makes an image of the echelle grating onto the cross-disperser; the ray is thus dispersed by the echelle just at the position of the cross-disperser for the following optical system. Since a re-imaging lens is placed near the cross-disperser, the diameter of the ray dispersed at the cross-disperser is still small at the re-imaging lens. Otherwise, an unfeasibly large aperture of the re-imaging lens is required in the case of a non-white pupil configuration. The re-imaging lens of NICE was designed as a relay optical system with a magnification of one-third, which converts the telescope F-ratio of 12.2 to a re-imaging lens F-ratio of 4.1, and also converts the slit widths of $90\ \mu\text{m}$ and $180\ \mu\text{m}$ to images of $30\ \mu\text{m}$ and $60\ \mu\text{m}$ on the detector, respectively. As a consequence, the combination of the semi-Littrow configuration with the small γ and the

Table 1. Principal optical parameters.

Item	Specification			
Spectroscopic mode				
Designation in NICE	I	J	H	K
Wavelength range	0.91–1.20	1.17–1.47	1.41–1.78	1.73–2.45
Wavelength resolution for 2 pixels	~ 2600			
Combination of filter and CD*	F-IJ + CD-J [†]	F-IJ + CD-J [†]	F-HK + CD-H	F-HK + CD-K
Slit width and length (")	1 × 6.7 or 2 × 6.7 [‡]			
Spatial resolution ("/pixel)	1.32 [‡]			
Infrared-imaging mode				
Optical magnification	0.55 × of telescope focal plane			
Spatial resolution	0.81/pixel [‡]			
Field of view	206.2" × 206.2" [‡]			
Wavelength range	0.9–2.4 μm (filters are shared with spectroscopic mode)			
Slit viewer				
Optical magnification	0.48 × of telescope focal plane			
Spatial resolution	0.145/pixel [‡]			
Field of view	148" × 111" [‡]			
Wavelength range	~ 0.5–0.8 μm			

* Names and specifications of filters and CDs are listed in table 2.
[†] Angles of inclination of CD-J are different between I and J.
[‡] Values in use of the 1.5 m telescope of National Astronomical Observatory of Japan.

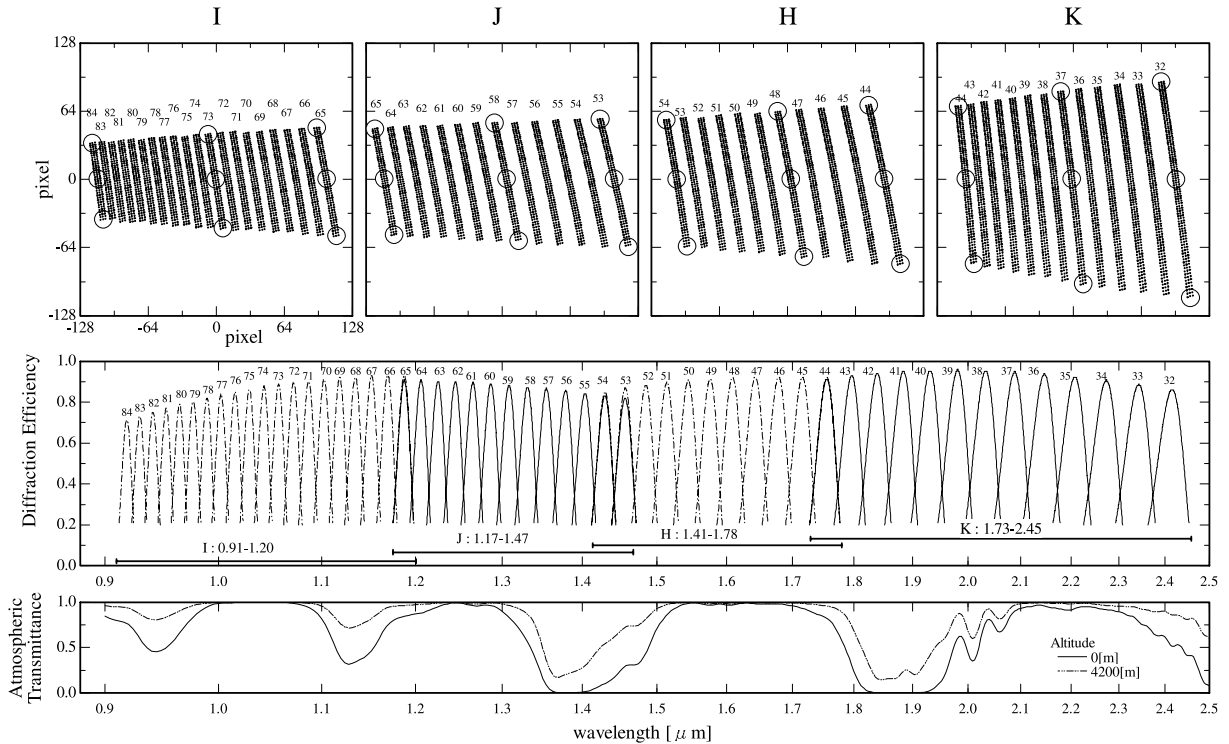


Fig. 3. Echelle formats and the diffraction efficiency with the echelle and the cross-disperser. The four upper panels show echelle formats of the I, J, H, and K frames. The order numbers are given in the figures at the top of the respective orders. The middle panel shows the diffraction efficiency with the echelle and the cross-disperser, and the wavelength coverages of the four frames. The lower panel shows the typical atmospheric transmittance. The whole wavelength range covered by NICE is divided into four frames at wavelengths inside the atmospheric windows with overlaps between the neighboring frames in order to combine the four-frame spectra accurately in the process of data reduction.

Table 2. Device specifications.

Device	Specification															
Spectroscopic mode																
Slit	Selectable from two slits. <ul style="list-style-type: none"> · $90 \times 600 \mu\text{m}$ for $1'' \times 6''.7$ · $180 \times 600 \mu\text{m}$ for $2'' \times 6''.7$ 															
Filter	Selectable from six filters on a filter wheel. <table border="1" style="margin-left: auto; margin-right: auto;"> <thead> <tr> <th>name</th> <th>wavelength (μm)</th> </tr> </thead> <tbody> <tr> <td>F-IJ</td> <td>0.8–1.5</td> </tr> <tr> <td>F-HK</td> <td>1.4–2.5</td> </tr> <tr> <td>K</td> <td>standard K band</td> </tr> <tr> <td>Bry</td> <td>2.16</td> </tr> <tr> <td>Open</td> <td>no filter</td> </tr> <tr> <td>Close</td> <td>black aluminated plate</td> </tr> </tbody> </table>	name	wavelength (μm)	F-IJ	0.8–1.5	F-HK	1.4–2.5	K	standard K band	Bry	2.16	Open	no filter	Close	black aluminated plate	
name	wavelength (μm)															
F-IJ	0.8–1.5															
F-HK	1.4–2.5															
K	standard K band															
Bry	2.16															
Open	no filter															
Close	black aluminated plate															
Semi-littrow	Refractive semi-Littrow configuration for the echelle grating with four elements. (S-FPL53 + S-TIH14 + BaF ₂ + CaF ₂) focal length = 114 mm															
Echelle	Gold coated reflective grating. 24.35 lines mm ⁻¹ blaze angle = 70° made by Spectra-Physics, Inc. effective aperture = $9.1 \times 26.7 \text{ mm}^2$															
Collimator	Refractive system with three elements. (BaF ₂ + S-TIH14 + CaF ₂) focal length = 240 mm															
Cross-disperser	Selectable from four CDs and a plane mirror on a CD wheel. <ul style="list-style-type: none"> · CDs are gold coated reflective gratings. <table border="1" style="margin-left: auto; margin-right: auto;"> <thead> <tr> <th>name</th> <th>lines mm⁻¹</th> <th>braze angle (deg)</th> </tr> </thead> <tbody> <tr> <td>CD-I</td> <td>600</td> <td>17.45</td> </tr> <tr> <td>CD-J</td> <td>400</td> <td>13.90</td> </tr> <tr> <td>CD-H</td> <td>300</td> <td>14.60</td> </tr> <tr> <td>CD-K</td> <td>150</td> <td>8.63</td> </tr> </tbody> </table> <ul style="list-style-type: none"> made by Spectra-Physics, Inc. effective aperture = D19.2 mm · A plane mirror is gold coated for infrared-imaging mode. effective aperture = 11.6×16.4 	name	lines mm ⁻¹	braze angle (deg)	CD-I	600	17.45	CD-J	400	13.90	CD-H	300	14.60	CD-K	150	8.63
name	lines mm ⁻¹	braze angle (deg)														
CD-I	600	17.45														
CD-J	400	13.90														
CD-H	300	14.60														
CD-K	150	8.63														
Re-imaging lens	Refractive system with five elements. (BaF ₂ + S-TIH14 + CaF ₂ + CaF ₂ + S-FPL53) focal length = 80 mm															
Detector	NICMOS-3															
Calibration lamp	Three lamps are available independently or simultaneously. <ul style="list-style-type: none"> · Kr and Ar for wavelength calibration. · Halogen to trace the echelle format. 															
Infrared-imaging mode																
Filter	Shared with spectroscopic mode.															
Collimator	Refractive system with three elements. (BaF ₂ + S-TIH14 + S-FPL53) focal length = 145 mm															
Re-imaging lens	Shared with spectroscopic mode.															
Detector	Shared with spectroscopic mode.															
Slit viewer																
Relay optical system	Achromatic with four elements in two groups. (SF5 + BK7 + SSKN8 + SF10) magnification = $0.48 \times$															
Detector	Bitran corp. BJ-32L type CCD 1024×768 pixels, $6.25 \mu\text{m}/\text{pixel}$															

ranges. The near-infrared rays reach the NICMOS-3 detector through a collimator for the infrared-imaging mode, a plane mirror substituted for the cross-disperser, and the re-imaging lens, while the optical rays enter into the slit viewer. Objects invisible in the optical wavelength range can be pointed with this infrared imaging mode (figure 1).

2.2. Mechanical System

The whole system, except for the calibration lamps and the slit viewer, is mounted on an optical bench in a cryostat shaped as a box. This box shape cryostat is tough enough to support the inner structure with negligible deflection.

In order to reduce the weight of the optical bench while keeping its deflection negligible, the optical bench consists of a thin aluminum plate and reinforcing plates, which are assembled so as to also make a box structure, named “cold-box”. The cold-box also works as a radiation shield. Since the optical parts are fixed on the optical bench with locating pins, we need no particular alignment process. The cold-box is cooled down to ~ 120 K to reduce the thermal background radiation, and the detector is cooled down to ~ 80 K to suppress the dark current. The optical bench and the detector are connected to a single-stage cooler (Daikin industries, Ltd., V102CL) with two individual copper wires to keep them at the different temperatures.

2.3. Detector and Data Acquisition System

We adopted a NICMOS-3, which has 256×256 pixels with $40 \mu\text{m}/\text{pixel}$, and covers the wavelength range from $\sim 1 \mu\text{m}$ to $2.4 \mu\text{m}$. The driving clock patterns for the NICMOS-3 are transferred from a MESSIA-IV CIC board (Sekiguchi et al. 1998) to a “Bias-Box” (manufactured by Infrared Laboratory, Inc.), and finally to the detector. The analog signal from the detector is amplified by a “Pre-Amp” (also, Infrared Laboratory, Inc.), and digitized by A/D boards (Hiromoto et al. 1995). GUI control software running on a Windows 2000 PC displays the obtained spectral images, the hardware status, and the observation log in real time.

3. Basic Performance

The read noise and the dark current are $30\text{--}40 e^-$ and $0.4 e^- s^{-1}$, respectively, at an operating temperature of 80 K. The conversion factor is $10.0 e^-/\text{ADU}$. The detector has a bad column at the center of the sensitive area. It causes large errors in the wavelength ranges of $\Delta\lambda \sim 0.01\text{--}0.02 \mu\text{m}$ in respective frames of I–K. The spectra of these wavelength ranges were removed by the data-reduction process.

The throughput of NICE was evaluated by comparing the observed spectra of A-type stars with calculated spectra from their brightness and spectral types. For example, the throughput estimated from observations of HR 5676 (A2 V) is shown in figure 6. The throughput of NICE, itself, with atmospheric transmittance ranges from 13% to 18% at the braze wavelengths in atmospheric windows.

The limiting magnitude was estimated from the noise level in the obtained spectra. The read noise was dominant in observations within 600s exposure, and made the limiting magnitudes to be 11.0 mag, 10.7 mag, 10.5 mag, and 10.3 mag

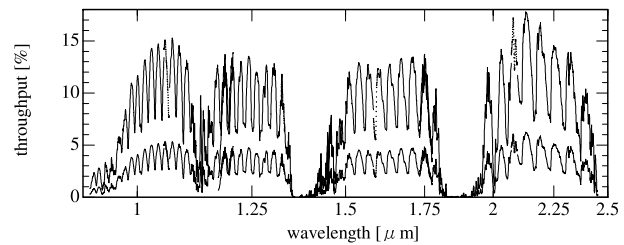


Fig. 6. Throughput of NICE evaluated based on a set of observations of HR 5676 ($m_V = 5.26$ mag, A2 V). The upper line indicates the throughput of NICE, itself, i.e., the optical transmittance and the quantum efficiency of the detector, with atmospheric transmittance. The lower one indicates the throughput, including a telescope transmittance of 70% and a light loss at the slit of 50%, in addition to the upper throughput.

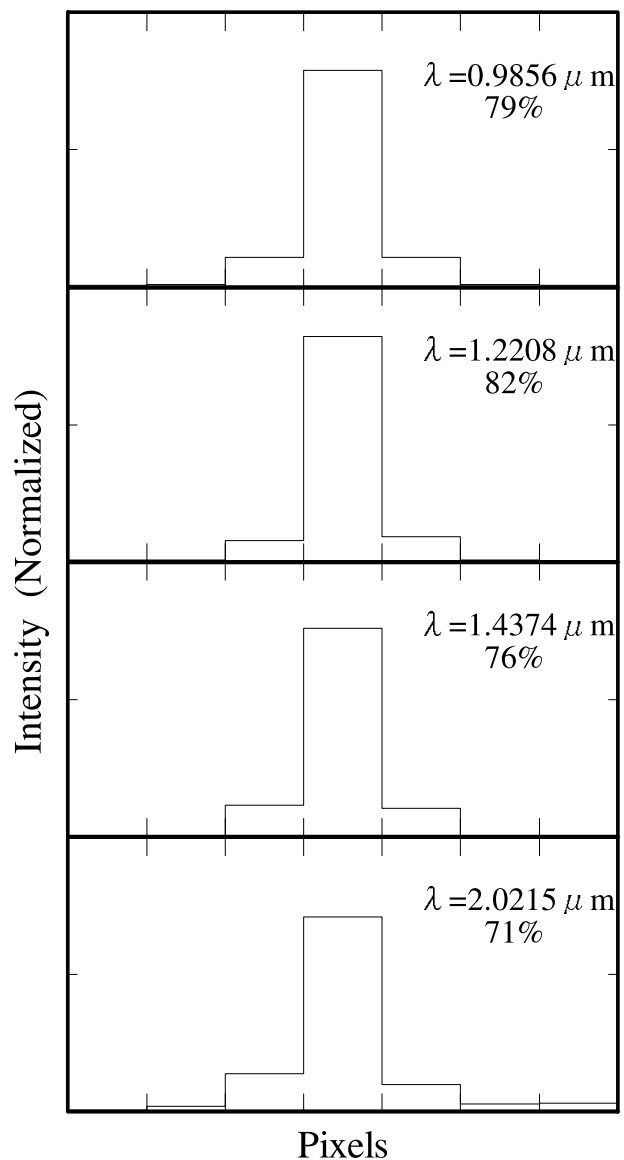


Fig. 7. Typical line profiles of a krypton lamp with a slit width of $1''$. The ordinate indicates the normalized intensity, while the abscissa is pixel. Each wavelength of the line is written with the percentage detected in a single pixel.

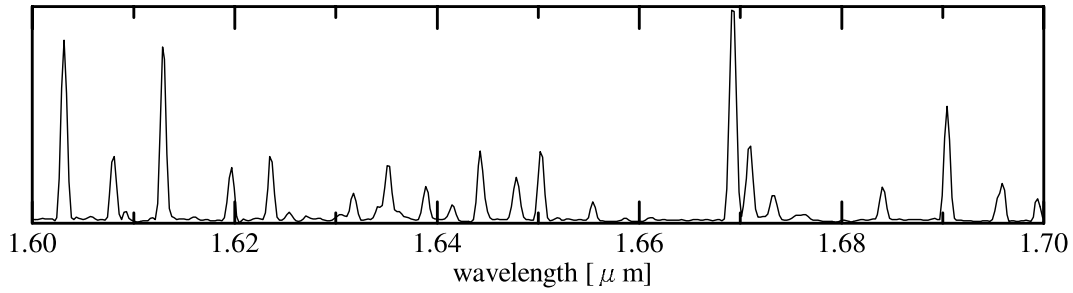


Fig. 8. Spectrum of OH airglow obtained with a slit width of 2". The ordinate indicates the relative intensity, while the abscissa is the wavelength.

Table 3. Targets and standard stars in the observations.

Target		A-standard		G-standard		Date	
HR 696	10 Per	B2 Ia	HR 1046	A1 V	HR 915	G8 III	2003.10.23
HR 7924	Deneb	A2 Ia	HR 8028	A1 Vn	HR 7328	G9 III	2002.08.20
HR 7518	SU Cyg	F2 I	HR 7736	A2 V	HR 7615	K0 III	2002.11.13,27
HR 3188	ξ Mon	G2 Ib	HR 3314	A0 V	HR 3212	G6 III	2003.01.21
HR 2580		K2 Iab	HR 2414	A0 V	HR 2311	K5 III	2004.01.13,14
HR 8383*	VV Cep	M2 Iaep	HR 8585	A1 V	HR 8688	K1 III	2003.10.23

* Eclipsing binary consisting of M2 Iaep and B8 Ve with magnitude difference of 1.7.

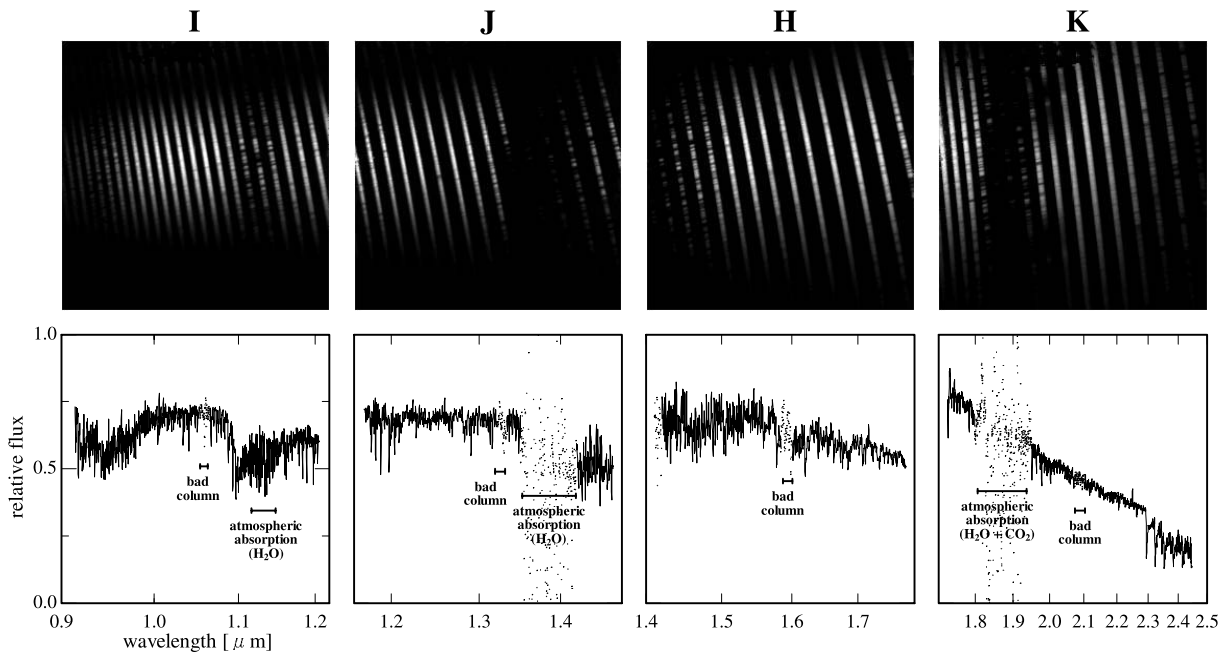


Fig. 9. Spectral images on the detector obtained in the I, J, H, and K frames (upper panels) and the reduced spectra (lower panels) of HR 2580 (K2 Iab). The spectral data with low S/N ratios due to the atmospheric absorption and the bad column of the detector are indicated with dots.

for the I, J, H, and K frames, respectively, with 10σ , 600 s exposure, a 2" slit, and a seeing of 1".

Typical profiles of emission lines taken with a 1" slit are shown in figure 7. More than 70%–80% of the flux for each line is concentrated in a single pixel. The full width half maximums (FWHM) of profiles estimated from thirty luminous krypton lines are 1.0 ± 0.2 pixel and 1.5 ± 0.2 pixel for slit widths of 1" and 2", corresponding to a wavelength resolution of

$\lambda/\delta\lambda \sim 5300$ and 3400, respectively. An obtained spectrum of OH airglow is also shown in figure 8 to demonstrate the wavelength resolution. The profiles of lines of OH airglow are well resolved owing to the resolution, according to the purpose described in section 1.

Since any stray light distributes smoothly on the detector, it can be reduced to less than 1% of the stellar signal by subtracting of the background fitted with a 5th-order

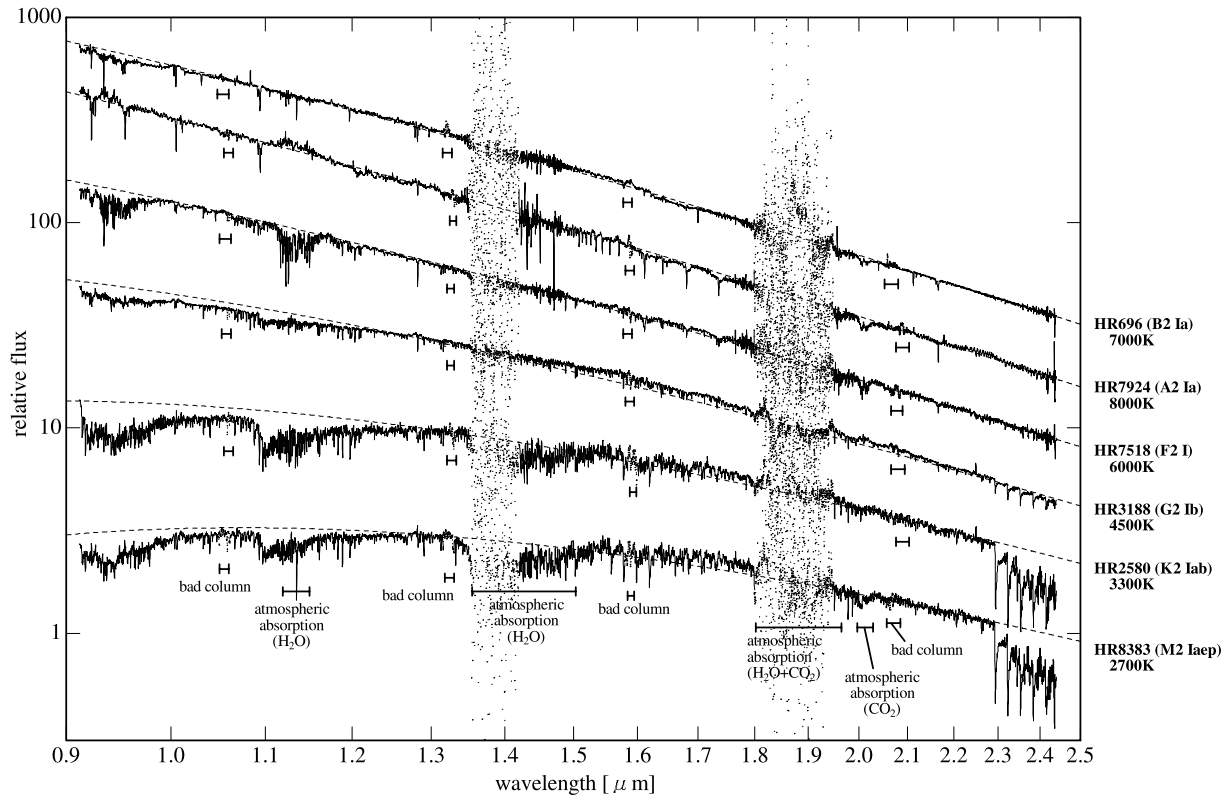


Fig. 10. Spectra of supergiants listed in table 3. Many jaggy patterns are originated from the stellar absorption lines. The blackbody spectra fitted at $1.3 \mu\text{m}$ and $2.2 \mu\text{m}$ are also shown by dashed lines. The temperatures of the blackbodies are written together with the HR numbers of the stars.

polynomial. No other remarkable ghosts are seen in the image.

4. Examples of Observations

In order to demonstrate the capability of NICE, we show several spectra of supergiants here (listed in table 3). Since supergiants have various shapes of continua and absorption lines, corresponding to their spectral types, they show the availability of NICE for the research of our observational project on massive stars.

A set of spectral observations consisted of a target star, standard stars, and calibration lamps. Two types of standard stars were selected from A0 V–A2 V stars (A-standard) and G6 III–K1 III stars (G-standard). The airmasses that we observed for the standard stars differed from those for the target stars by no more than 0.12. The spectra of sky neighboring the target and the standard stars were obtained just before and after the exposure of the stars. The spectra of the krypton and the argon lamps for wavelength calibration, and that of the halogen lamp for tracing the echelle formats on the detector were also obtained. Since these images for the calibration were taken in a set of each observation within one hour, the wavelengths were accurately calibrated with an error of less than 0.3 pixel. Four sets of the above-mentioned observations for the I, J, H, and K frames were made to obtain complete spectra between $0.9\text{--}2.4 \mu\text{m}$.

The data were reduced with the echelle package of IRAF.¹

At first, for a single-frame, e.g., I frame, the sky frame was subtracted from the target frame, and any bad pixels were corrected. Second, the stray light and the fluctuation of the bias level were subtracted with a 5th-order polynomial fitted to the area of the background, except for the spectral image. Third, the frame was rotated 12° to adjust the inclination of the slit image on the detector. Fourth, the individual echelle orders were cut out from the frame, and the data were correlated with the wavelength by using the krypton and argon spectra. Fifth, many orders were combined to make a single-frame spectrum, e.g., I frame spectrum. These procedures were also done for the spectra of A-standard and G-standard stars. Then, parts of the spectra around the hydrogen absorption lines of the A-standard star were replaced to those of the G-standard star. The spectrum of the target star was divided by that of the hydrogen-replaced A-standard star, and then multiplied by a blackbody spectrum with a temperature corresponding to the spectral type of the A-standard star. The same procedures were repeated for the J, H, and K frames. Finally, the entire spectrum between $0.9 \mu\text{m}$ and $2.4 \mu\text{m}$ was created by combining the I, J, H, and K frame spectra. Since the spectra of the two neighboring frames overlap each other, it was easy to combine the four spectra with high accuracy. For example, the four spectra in the four wavelength ranges of a K2 Iab star, HR 2580, are shown in figure 9. The combined spectrum is exhibited in figure 10 together with those of the other target

¹ Distributed by the National Optical Astronomy Observatory, and operated

by the Association of Universities for Research in Astronomy, Inc., under contract with the National Science Foundation.

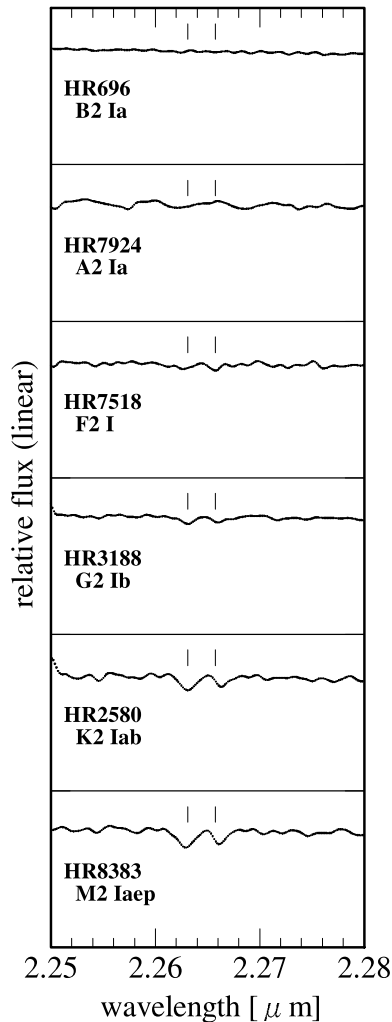


Fig. 11. Spectral profiles of the Ca I absorption lines at 2.2631 μm and 2.2657 μm obtained with a slit of $2''$.

stars listed in table 3. The error in the combining process is estimated to be smaller than 3% of the continuum level.

For the six combined spectra of B2–M2 supergiants in figure 10, evaluation of the continuum levels is fairly easy and accurate. The blackbody spectra fitted at 1.3 μm and 2.2 μm are also shown with dashed lines in figure 10. As a result of accurate fittings, weak excess at $\sim 1.6 \mu\text{m}$ caused by the H^- opacity minimum, can be seen especially in the K2 I–M2 I spectra. Many absorption lines are resolved thanks to a wavelength resolution of $R_{2\text{pix}} \sim 2600$. As shown in figure 11, the resolving power is demonstrated by the well resolved profiles of the Ca I absorption lines at 2.2631 μm and 2.2657 μm , whose separation is only 0.0026 μm . These data demonstrate that NICE is a powerful instrument for not only evaluating the continuum levels, but also for detecting spectral lines without blending.

We thank Dr. Hirokazu Kataza for providing the A/D boards, and Dr. Shin-ichiro Okumura for information concerning detector operation. We also thank Dr. Kunio Noguchi for his careful reading of this manuscript. We are grateful to the referee for his comments to improve our manuscript. We are also grateful for support from Toray science foundation development aid.

References

- Baranne, A., et al. 1996, A&AS, 119, 373
 Hiromoto, N., Takami, H., Aoki, T., Kataza, H., Yamashita, T. & Sato, S. 1995, PASJ, 47, 93
 Maihara, T., Iwamuro, F., Yamashita, T., Hall, D. N. B., Cowie, L. L., Tokunaga, A. T., & Pickles, A. 1993, PASP, 105, 940
 Oliva, E., & Origlia, L. 1992, A&A, 254, 466
 Rousselot, P., Lidman, C., Cuby, J.-G., Moreels, G., & Monnet, G. 2000, A&A, 354, 1134
 Schroeder, D. J. 2000, *Astronomical Optics* (San Diego: Academic Press), chapter 14–15
 Sekiguchi, M., Nakaya, H., Kataza, H., & Miyazaki, S. 1998, *Experimental Astron.*, 8, 51
 Yamamuro, T., Nishimaki, Y., A. Letip, Motohara, K., Miyata, T., & Tanaka, M. 2006a, PASJ submitted
 Yamamuro, T., Sato, S., Zenno, T., Takeyama, N., Matsuhara, H., Maeda, I., & Matsueda, Y. 2006b, *Optical Engineering*, 45, 083401